Design and testing of an in-flight thrust measurement system for a pylon-mounted miniature jet engine

Julius Bartasevicius*, Pedro Alexandre Tonet Fleig†, Annina Metzner‡ and Mirko Hornung§
Technical University of Munich, Boltzmannstrasse 15, 85748 Garching

Optimization of aircraft's performance often requires careful consideration of aerodynamic drag. However, direct measurement of drag of a flying vehicle is not feasible. Therefore, in order to measure the change in drag for different configurations of a flying aircraft, in-flight thrust measurement is necessary, which can consequently be used to derive drag. For this reason, the design of an in-flight thrust measurement system for a pylon-mounted jet engine is presented. The system is based on the trunnion thrust method. The design process is described, including a review of state of the art as well as measurement error consideration. Calibration methods are presented. During the calibration, the thrust root-mean-square error of 0.64 N was observed. The system was flight tested and proved to work reliably in real-life conditions. Finally, the flight test data was used to generate a thrust model based on engine parameters.

I. Introduction

It is not feasible to directly measure aerodynamic drag in-flight. Therefore, to quantify any changes in drag on a flying aircraft, knowledge about the other forces acting on it, namely lift, weight and thrust, is required. This work presents the design of a thrust measurement system for a miniature jet engine within the framework of the project FLiPASED (Flight Phase Adaptive Aero-Servo-Elastic Aircraft Design Methods, `https://cordis.europa.eu/project/id/815058`).

One of the goals of the project FLiPASED is to reduce the induced drag in-flight. This will be done by optimizing control surface deflections, which in turn changes the load shape distribution over the wings. The reduction of induced drag will be shown in-flight with the help of a subscale flight demonstrator (SFD) T-FLEX which has been developed for the predecessor project, FLEXOP (Flutter Free Flight Envelope Expansion for Economical Performance Improvement, `https://flexop.eu/`). Within the FLEXOP project a 65 kg take-off weight, 7 m wingspan swept wing unmanned aircraft was designed and built [1].

As the change of the induced drag is expected to be within 2-5% [2], accurate knowledge about the thrust provided by the engine is required. Consequently, to supplement the thrust data from an already available engine model [3], additional in-flight measurements are required. This is achieved by implementing a load-cell based thrust measurement system that can measure the applied thrust with an accuracy of 2%. The correct functioning of the system is key for validating the drag reduction measures within the FLiPASED project.

Within this work a review of existing methods for thrust measurements with focus on applications for subscale demonstrators will be presented (section II). System requirements and design process applied to T-FLEX SFD will be described (section III), as well as calibration procedures (section IV) and the in-flight measurement results (section V).

II. State of the art

The existing thrust measurement methods are discussed here. Section II.E focuses specifically on methods that have been applied to measure thrust of miniature engines commonly used to power unmanned vehicles.

A. Gas generator method

The gas generator method uses the measurements taken inside the engine (mass flow, pressure or temperature) to derive the thrust. These are taken at various stations of the engine (commonly nozzle and inlet) and allow gross thrust derivation [4]. The main disadvantage of this method is that it requires multiple sensors installed within the engine.

*Research Assistant, Chair of Aircraft Design, Boltzmannstrasse 15, 85748 Garching, Germany, julius.bartasevicius@tum.de
†Alumnus TUM M.Sc. Aerospace, Chair of Aircraft Design, Boltzmannstrasse 15, 85748 Garching, Germany, pedroafleig@outlook.com
‡B.Sc. Engineering Science, Chair of Aircraft Design, Boltzmannstrasse 15, 85748 Garching, Germany, annina.metzner@tum.de
§AIAA Senior Member, Professor, Head of the Chair of Aircraft Design, Boltzmannstrasse 15, 85748 Garching, Germany, mirko.hornung@tum.de

While this might not be a problem for power plants used on manned aircraft, implementation of additional sensors in the miniature engines becomes more complex.

B. Brochure method

The brochure method is considered the simplest thrust measurement technique in terms of required measurements and installed equipment [4]. It can be implemented, for example, using only the rotational speed of one of the shafts as an input. However, this method requires extensive tests and calibration, usually performed by the engine's manufacturer to create data tables that correlate certain parameters with the generated thrust. Therefore, the brochure method, while reliable and accurate when sufficient data and additional engine parameters are available for validation, is less suitable for a small-scale engine. This is mainly due to the following reasons: Firstly, there is usually very limited test data provided by the engine's manufacturer. Secondly, due to non-existent certification requirements for such engines, higher deviations between two engines of the same type can be expected.

C. Swinging probe method

The swinging probe method uses calibrated sensors traversing the engine's exhaust nozzle to perform total and static pressure, total temperature, and flow direction measurements [4]. In some cases, multiple sensors are placed in rakes to obtain better results, as shown by Davidson [5] in an application that was able to measure the net thrust. This configuration of the probes has the advantage of not requiring provisions for their installation in the engine's core, because all sensory is placed on the outer side. However, as the sensors and mountings are within the high pressure and temperature area behind the engine, the complexity and cost of the measurement system is high.

D. Trunnion thrust method

The most direct method for measuring thrust requires no pressure, temperature, or airflow sensory. Instead, the trunnion thrust method directly measures the force imposed by the propulsion unit on its mounting structure [4]. This makes the technique particularly attractive when using thrust for drag computations, because the force vector created by the propulsion unit can be measured directly.

However, aircraft engine attachments are complex structures. These are often statically indeterminate and have more than the minimum number of support points to ensure higher safety levels. Moreover, they not only contain load bearing parts, but also wires, pipes, and hoses which can affect the load measurement performed on the supports. Accordingly, the trunnion thrust method is considered unfeasible for large aircraft [4]. Nevertheless, experiments have been performed successfully. For instance, the tests performed in Conners and Sims [6] were able to obtain thrust values in a supersonic aircraft implementing direct measurements. Muhammad et al. [7] has developed a system with this technique for a propeller-driven aircraft and obtained values that were in accordance with other thrust measurement methods tested. This work also emphasized the importance of Finite-Element Method (FEM) analysis to ensure an optimal placement and geometry of load cells and strain gauges.

E. Thrust measurement of miniature engines

Most of the methods mentioned above were developed for manned aeroplanes with engines that went through extensive certification procedures and tests. In contrast, in the unmanned aviation many propulsion components are high-grade radio-controlled model engines with minimal performance data sheets and low or non-existent standards for certification. Therefore, interested users have to perform the engine performance analysis on their own. Some of such examples are given below.

Martinez [8] investigated methods to measure the thrust of a miniature jet engine integrated within an airframe. It included an extensive analysis to determine the best cell geometry and strain gauge positioning to eliminate the influence of lateral and vertical forces that could affect in-flight readings. The final design was a pair of horizontal metal holders instrumented with strain-gauges. Unfortunately after installation it was discovered that the thermal expansion of the engine influenced the measurements too much [9].

Simavilla [10] has also designed a system based on load cell force measurement. Its sensor placement and attachment reduced the heat-induced effects. Moreover, this design highlighted the requirement of a well-defined and compatible load path for the chosen sensor configuration. As a result, the presented solution used a hinged assembly in one of the engine attachment points and achieved 1% measurement accuracy for a $90N$ power-plant.

Bronz et al. [11] measured thrust by Gaussian fusion of two methods: a pre-calibrated motor in the wind tunnel (based on an airspeed estimate) and a direct force measurement sensor. The direct force measurement was done with a thin-film force sensor which was integrated within the motor mount. This sensor proved sensitive to the vibrations generated by the propeller, which significantly increased signal noise.

Sartori and Yu [12] investigated thrust measurement for a quadrocopter equipped with brushless electric motors and plastic propellers. They identified the problems within the usual Blade Element Theory approach and proposed an approach which, by experimentally measuring additional propeller parameters, improves the thrust estimation.

Bergmann et al. [13] presents an on-board thrust measurement system applied on an electrically-powered propeller UAV. The concept uses a load-cell placed in between the airframe and the electric motor. Tension and torque are measured by the load-cell. While the authors note that the accuracy of the concept was demonstrated under lab conditions, high deviation of measured in-flight thrust is reported, which is attributed to the fluctuations in propeller speed.

III. System design

A. Description of the demonstrator

The T-FLEX technology demonstrator is a jet-engine-powered UAV with 65 kg take-off weight and 7 m wingspan (Fig. 1). The UAV is flown manually by pilot via external vision. Rate control flight mode is used, where surface deflections are directly linked to the joystick positions on the transmitter. The autopilot is used only during some test sequences, but not during take-offs or landings.

Fig. 1 T-FLEX Subscale flight demonstrator during landing phase.

The aircraft is equipped with integrated measurement equipment. Air data (aerodynamic angles, airspeed and pressures), position (GPS coordinates) and inertial parameters (accelerations, attitude angles) are being logged on the aircraft. In addition, wings are equipped with multiple inertial measurement units spaced along the wingspan for vibration measurement.

The geometry of the aircraft is summarized in Table 1.

For further background on flight test operations of the T-FLEX demonstrator see Bartasevicius et al. [14].

Table 1 Geometry of FLEXOP UAV.

Wing span, m:	7.07	Tail projected span, m:	1.27
Wing area, m^2:	2.53	Tail area, m^2:	0.39
Wing aspect ratio:	19.74	Tail aspect ratio:	4.2
Wing incidence, deg:	-0.52	Tail incidence, deg:	-4.33
Wing 0.25c sweep, deg:	18.36	Tail 0.25c sweep, deg:	19.83
Wing taper ratio:	0.5	Tail taper ratio:	0.52
Wing twist, deg:	-2	Tail dihedral, deg:	35
Number of wing control surfaces:	8	Number of tail control surfaces:	4
Fuselage length, m:	3.42		
Fuselage maximum height, m:	0.315		
Fuselage maximum width m:	0.3		

B. Jet engine description

The main requirements while designing the propulsion system for T-FLEX were high acceleration, low vibration and precise speed tracking [15]. Taking these requirements into account, a jet engine paired with a fast-response airbrake system [16] was selected. The jet engine is a BF B300F turbine with 300 N maximum thrust capability. The engine was mounted on a pylon above the fuselage with the fuel tank located directly below it with the intent to keep the same centre of gravity throughout the flight.

The engine is round in shape and is secured to the aircraft via a steel-cage (Fig. 2). The cage is mounted on four aluminium holders attached to the main propulsion rack structure made out of carbon-fiber-reinforced polymers (CFRP) plates.

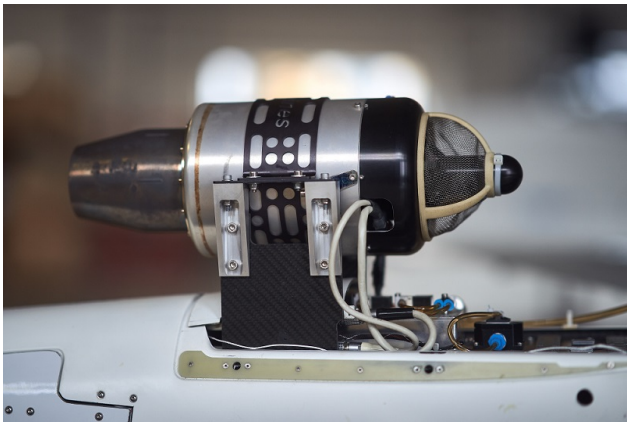

Fig. 2 Mounting of the BF B300F turbine on the aircraft.

C. Design requirements

The intentions of designing a thrust measurement system were to improve the available data for flight model identification [17] and to allow quantification of the drag reduction when active wing shape control is used. The expected overall drag reduction is in the order of 2 to 5%, which for cruise flight results in 1 N to 3 N. The lower limit of 2% was taken as the required accuracy for the thrust measurement system.

The system was also required to have a measurement range over the whole available thrust envelope (0 N to 300 N) and for the complete duration of flight (minimum of 30 minutes). Due to the slow dynamics of the jet turbine and therefore no fast changes in thrust values, a minimum sample rate of 50Hz was chosen.

Environmental conditions also had to be taken into account. Temperature, altitude and pressure as well as weather-induced conditions such as wind and rain were to be expected. Additionally, it had to be possible to compensate

the measurements for off-level flight condition. Measurement of net thrust was required.

Table 2 summarizes the requirements.

Table 2 Summary of design requirements for the thrust measurement system.

Sub-Requirement	**Value**
Range of Measurement	$0 \leq T \leq 300$ N
Precision of Measurement	$\pm 2\%$
Duration of Measurement	≥ 30 minutes
Sample Rate	≥ 50 Hz

D. Design process

The design process started with a study of the applicability and feasibility of the previously reviewed thrust measurement methods.

While the gas generator and swinging probe methods were assumed to have the best potential for accuracy, these would need the most complex instrumentation. For the gas generator method, pressure and temperature probes would have to be installed within the engine itself. Thus, engine frame disassembly and modification would be required. This was not deemed possible with the available resources. In comparison, the implementation of the swinging probe (or rake) method, which uses sensors outside the engine, would be possible, but the high cost of temperature-resistant components was considered a disadvantage.

As the turbine was mounted on a pylon with four aluminium supports connected to two CFRP frames, the trunnion thrust method was chosen. This convenient engine mount would allow for more degrees of freedom to implement the force sensor, and the symmetry of the assembly would make the load paths clearly defined. Additionally, no engine modification would be necessary, and the sensor was expected to not significantly influence the aerodynamics of the aircraft.

The chosen method was implemented in two concepts described in the following sections.

1. Initial concept

The initial concept was based on substituting half of the engine's aluminium support brackets with load cells (Fig. 3a)[18]. The idea behind the concept was to achieve sufficiently low stiffness on the load cells for higher measurement accuracy while the bulk of the load would be carried through the original attachments. Thus, FEM analysis was performed to demonstrate that the forces at the sensors would be within their rated range and that the system would have sufficient stiffness for safety.

The system was tested with the calibration methods described in section IV. During the calibration, it became clear that the system did not deliver satisfactory accuracy and reliability. Two main issues were identified.

Firstly, the high temperatures from the jet engine had an influence on the load cell performance despite their rating for temperature compensation. Such effect was, similarly to the design in Martinez [8], due the thermal expansion of the cage that led to additional lateral forces interfering with the measurements. Stiffening the attachment points by additional longitudinal elements, as well as including heat-isolating spacers in between the heated steel cage and the load cells improved the results.

Secondly, the concept did not provide repeatable measurements. During calibration, it was observed that the measurement system had hysteresis loops. It was contemplated that the load paths would change when high thrust values are applied. Therefore, further improvements of the system were needed.

2. Final concept

The issues encountered with the initial concept were addressed with two core approaches. First, the point of measurement was centralized and placed in the aircraft's symmetry plane. This decoupled the effects of the engine's cage thermal expansion from the measurements. Second, the structure was made statically determinate to reduce the number of unknown support reactions and to provide a clear definition of the loads measured.

The simplest solution for such structure would be a single-point, clamp-style attachment with the load cell placed between the engine mount and the rest of the aircraft. However, this configuration would have both the reaction moment

over the aircraft's pitch axis and the reaction force in the longitudinal axis influencing the measured output. Therefore, to accurately obtain the thrust from the measurements, a multi-axial load cell would be required. It was decided that such a requirement would make the load-cell and its measurement corrections too complex. Therefore, another solution was required.

A solution with two attachment points and a simple single-axis load cell was adopted (Fig. 3b and Fig. 4). It is, in part, similar to the design presented by Simavilla [10] as the engine mount was also assembled on a freely rotating hinge. The main difference is that the found solution would use a single centrally placed load cell instead of two mounted on the sides of the engine. Moreover, the sensor would be installed within a rod with heim joints on both ends. This constitutes a support that transmits reactions only in the longitudinal direction, corresponding to the free body diagram shown in Fig. 4.

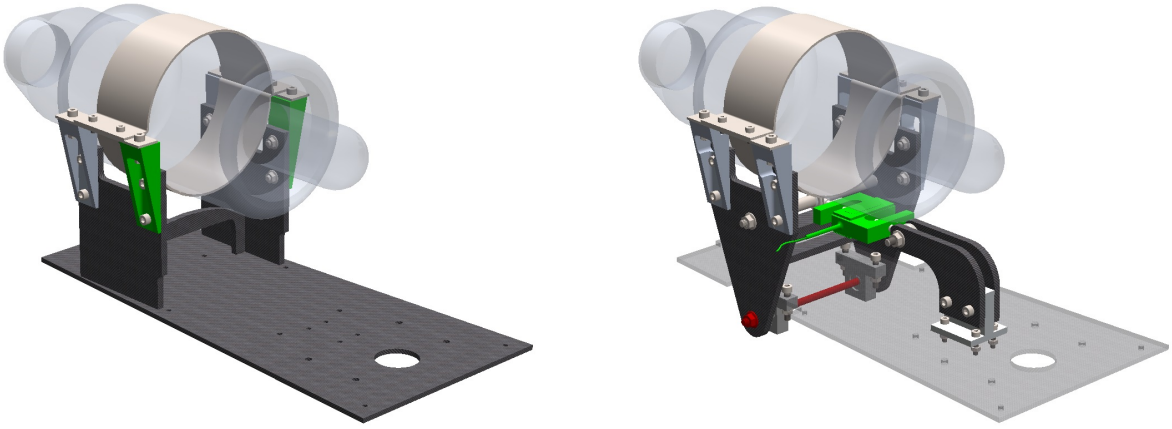

(a) Original propulsion stack. The support brackets, that were replaced by the load cells in the initial concept, are marked in green.

(b) The final version of the thrust measurement system. The load cell is marked in green and the hinge axis in red. The propulsion stack base plate is made transparent for clarity.

Fig. 3 Models of the initial and final propulsion stacks.

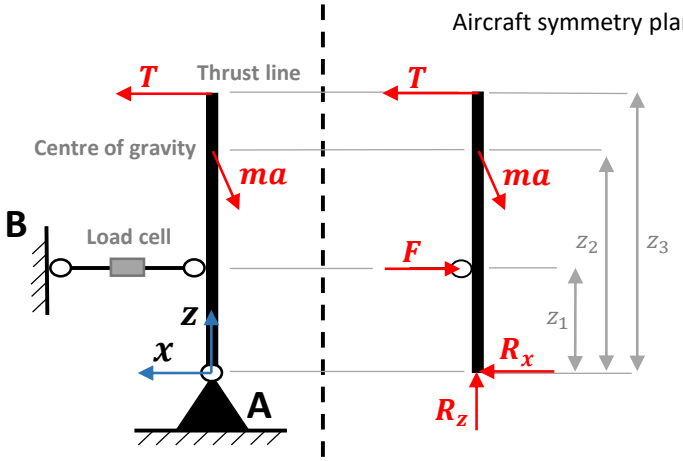

Fig. 4 Free-body diagram of the final concept in an accelerating state.

Two bending moments had to be balanced by the load cell to retain equilibrium. The main moment is due to the thrust vector created by the engine. The secondary moment that was considered was the one created by the accelerating or decelerating hinged assembly. Therefore, the moment balance equations are:

$$\sum M_A = 0 \tag{1}$$

$$-Fz_1 - ma_x z_2 + ma_z x_2 + Tz_3 = 0 \tag{2}$$

Here, F is the force measured by the load cell, m is the mass of the hinged assembly (the mass of fuel was ignored), a_x and a_z are the vertical and longitudinal accelerations of the hinged assembly and T is the thrust. z_1, z_2 and z_3 are vertical distances from the hinge point A and x_2 is the horizontal distance of the CG from the hinge line. As its value is very small, it is ignored in Fig. 4.

It was assumed that the deflections of the load cell are small and that the engine assembly and the aircraft fuselage can be treated as a single rigid body. Therefore, the accelerations measured by the main inertial measurement unit were transformed into the coordinate system of the CG of the hinged assembly and used for further corrections.

To further verify the rigid body assumption and to verify the direction of thrust vector, deflections of a loaded final system around the hinge axis were measured with a 3D scanner. Initially, the deflection angle at maximum load was found to be about three degrees. It was also observed that part of this deflection comes from the deformation of the base plate. Consequently, the base plate was reinforced with longitudinal stringers. The improvement of the structure reduced the deflection angle to one degree at maximum load. As most of the measurements would take place during steady flight with medium thrust setting, no further corrections were made for the deformation.

3. Selection of the load cell

Choosing the load cell was an integral point for the mechanical design of the system. The design variables like load cell capacity, the location of the hinge axis, the distance of the thrust line from the hinge axis and location of the load cell all influence each other. Therefore, an approach to manipulate these variables with the overall goal to reduce possible system errors was adopted.

Due to their good accuracy and low drift characteristics, strain-gauge based load cells were assumed the most appropriate for the design. Initially, bending beam, s-beam and single point load cells were considered. In the end, mainly due to their shape and mounting possibilities within our existing propulsion rack, an s-bend load cell was chosen. Options from four manufacturers were analysed, focusing on features such as thread size, thermal compensation, load rating and linearity. Table 3 lists some of the analyzed models and features.

Table 3 Load cell options

Model	**Non-Linearity**	**Temperature**	**Thread**	**Capacities up to 1kN**
InterfaceForce SSM	0.05 % F_{nom}	$-15 - 65°C$	M6	200,500,700,1000 N
HBM S2M	0.02 % F_{nom}	$-10 - 45°C$	M8	10,20,50,100, 200,500,1000 N
Althen / TE FN9620	0.05 % F_{nom}	$-10 - 45°C$	M12	500, 1000 N
ME-Systeme KD80se	0.05 % F_{nom}	$-10 - 70°C$	M8	100,200,500,1000N

The model InterfaceForce SSM[19] offered most rating options between 0.5 kN to 1 kN, which was the estimated required range. It was also among the two with the highest temperature compensation range while maintaining similar linearity characteristics to most others. Also, the smaller thread size allowed for smaller and lighter components which helped reduce overall structure weight.

To estimate errors of different configurations, a design algorithm was used. The following design inputs were taken into account:

- Allowable distance between the hinge axis and the thrust line
- Allowable distance between the load cell mounting point and the thrust line
- Accuracy data for the chosen load cell model as provided by the manufacturer
- List of available capacities of the load cell of the chosen model
- Desired safety margin between maximum force and load cell capacity
- Maximum thrust force value that the system should measure
- Thrust force value at which error estimation shall be performed
- Maximum expected temperature of the load cell during operation

• Minimum expected temperature of the load cell during operation

As a result, the measurement error was calculated:

$$\begin{aligned} < \epsilon_{abs} >= (< \epsilon_{nl} > + < \epsilon_{hyst} > + < \epsilon_{T0} >< \delta T >) < R > \\ +(< \epsilon_{rep} > + < \epsilon_{cr} > + < \epsilon_{T1} >< \delta T >) < F > \end{aligned} \tag{3}$$

Here ϵ are errors due to non-linearity (ϵ_{nl}), hysteresis (ϵ_{hyst}), temperature influence on zero-load value (ϵ_{T0}) and output value (ϵ_{T1}), repeatability (ϵ_{rep}) and creep (ϵ_{cr}). δT is the temperature difference, R is the rating of the load cell and F is the applied load. Resulting value ϵ_{abs} is the absolute measurement error.

In the end, a load cell with 700 N rating was chosen. The resulting positioning offered enough clearance for all existing components and cabling, reduced the maximum forces on the rest of the structure and allowed for easier assembly than if the load cell was placed closer to the engine. Additionally, the gap in between the engine and the load cell reduced the possibility of temperature influence from the engine.

The components required for the thrust measurement system to function added 0.6 kg of additional mass to the propulsion stack. Logging system is not included in this mass.

4. Logging system and signal processing

The data acquisition system consists of a model NAU7802 amplifier integrated with an analog-to-digital converter (ADC). This device provides an excitation voltage of 4.5 V to the load cell and has a maximum sampling rate of 320 samples per second. The amplifier is connected via I2C bus to an Arduino Nano, which is used to convert the data from I2C to USB and then sent to a Raspberry Pi where it is logged. So far, the created log file is not automatically synchronized to the main flight log. Therefore, synchronization is done manually by cross-correlating the aircraft pitch angle and measurements by the load cell during a pre-flight calibration (section IV.C). In the future, the synchronization of the two data logs will be done automatically.

The raw signal logged from the load cell had to be processed. First, the data had to be down-sampled using spline interpolation to fit the flight log from the main on-board computer which had a 200 Hz sampling rate. Then, building on the assumption that the engine thrust has a slow dynamics, the moving average filter was applied with a window size of 100 samples. This process is visually presented in Fig. 5 in both time and frequency domains. At the time of writing the nature of the oscillations of the raw signal are not yet investigated.

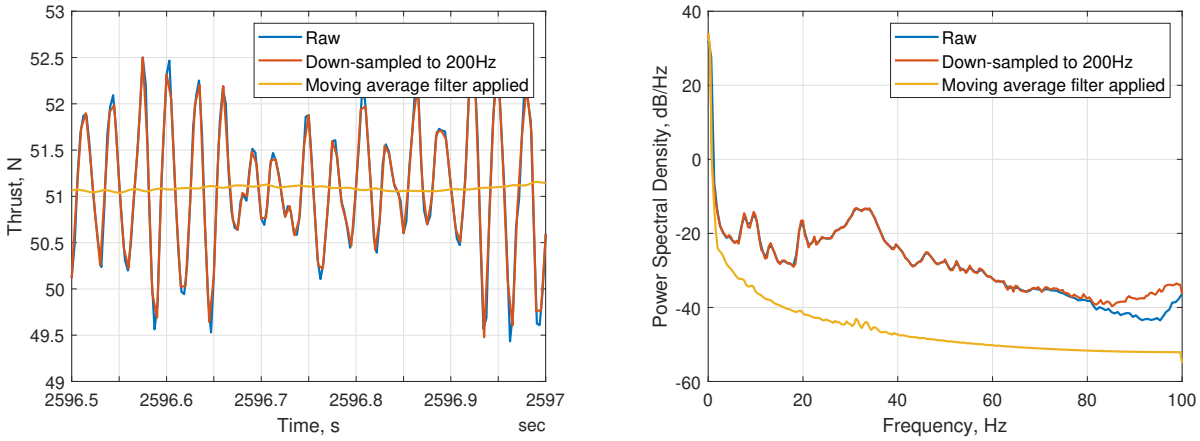

(a) Signal processing applied on flight data during a steady flight segment.

(b) Welch's power spectral density estimate graph of the complete flight during the signal processing steps.

Fig. 5 Process of processing the raw signal from the load cell.

The smoothing was also performed on the accelerations, which were required to extract the thrust. At that point the sensor signal was converted into physical units.

For further details on thrust measurement system design see Fleig [20] and Metzner [21].

IV. Calibration of the system

A calibration was needed to convert the raw sensor measurement into physical units. Calibration with weights was used as the main laboratory calibration environment. Furthermore, two methods to check and confirm a valid calibration were applied: calibration in the static propulsion test stand with a running engine and checking the calibration just before the flight by tilting the aircraft in engine-off condition.

A. Calibration with weights

For the calibration with weight blocks the system was mounted vertically. A wooden plate with a hook was installed as shown in Fig. 6. The weight blocks were hung on the hook and weight force, acting at the thrust line of the engine, was measured. In order not to damage the load cell, weights from 0 N to 350 N were used.

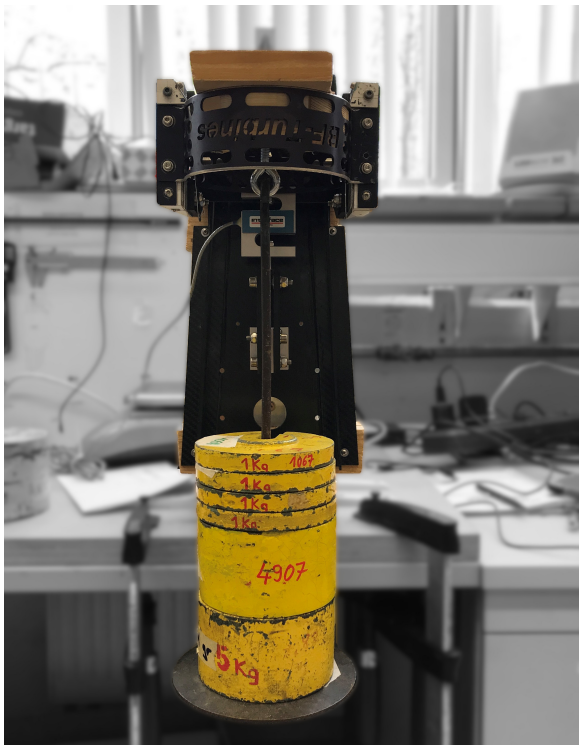

Fig. 6 Thrust measurement system is mounted vertically during the calibration.

The weight of the engine mount assembly was taken into account during calibration. The weight force was assumed to act straight down.

The weights in steps of 1 kg or 5 kg were applied in a random fashion. It was allowed for system to stabilize for two minutes and then a measurement of twenty seconds was taken.

Results were analyzed using Eq. 2 and plotted (Fig. 7). Three fit models were tested: ordinary least squares, robust linear regression (both of form $y(x) = bx + c$) and robust quadratic regression ($y(x) = ax^2 + bx + c$). Here x is the sensor value and y is the load, measured by the load cell in Newtons. In robust regression methods the outliers were identified using a bisquare weighting function and excluded from fit. This was assumed a valid step as no discontinuities in the calibration were expected.

All three methods provided accurate results, with robust linear fit having the lowest root-mean-square error of $RMSE = 1.24N$. Even though the 8 identified outliers were hardly visible in the calibration curve, the residuals of those test points deviate in between $2N$ and $6N$. No considerable benefit of using a quadratic fit was found. The coefficients of the different models are presented in Table 4.

It has to be noted that the errors reported above are for the loads as measured by the load cell. When extracting the thrust from the load cell measurements, the difference of lever arms in between the load cell and the thrust line have to be taken into account (Eq. 2). Therefore, when considering the accuracy of the measured thrust, these errors would have to be almost halved, resulting in $RMSE = 0.64N$.

Table 4 Comparison of three fitting methods to extract the calibration curve for the system. Coefficients of $y(x) = ax^2 + bx + c$ are summarised. Here x is the sensor value and y is the load, measured by the load cell in Newtons.

	RMSE, N	a	b	c	Outliers
Ordinary Least Squares:	1.69	0	-1.017e-04	1702	Included
Robust Linear Regression:	1.24	0	-1.019e-04	1705	Excluded
Robust Quadratic Regression	1.31	-1.347e-13	-9.826e-05	1681	Excluded

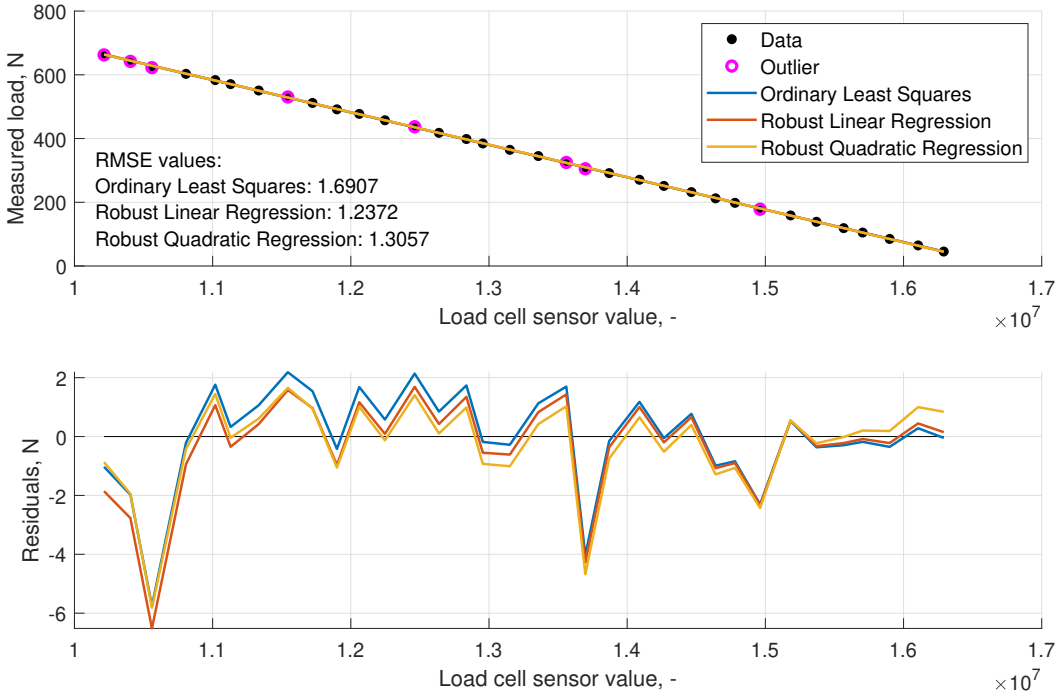

Fig. 7 Calibration curve of the load cell (top) and the residuals in between the measurements and the different fit models (bottom).

B. Calibration check on a static test stand

The calibration of the system was further validated with static thrust tests. The goal was to confirm the reliability of the calibration and investigate any temperature or vibration effects that may be caused by the jet engine.

The thrust measurement system was mounted on the turbine test stand of the Chair of Aircraft Design (Fig. 8). The stand features a Kistler dynamometer of model 9366cc with amplifiers of model 5073A. It is operated via Labview software. The recorded data had to be manually correlated in time, as no synchronization in between the two logging systems was available.

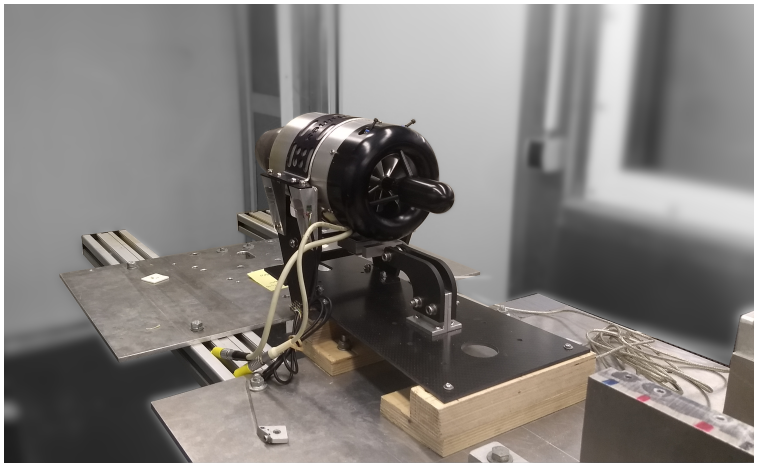

Fig. 8 Thrust measurement system mounted on a static propulsion test stand during calibration check. The dynamometer of the static test stand is located under the steel base plate.

A six minute test was done with a thrust profile similar to the one in-flight. The test stand was tared just before the measurements. It has to be noted that the test on the test stand was done before mounting the longitudinal stringers to stiffen the base, whereas the calibration curve applied to the measurements was extracted from measurements with the stringers.

Good correlation between the two measurement methods was observed (Fig. 9a). All changes of throttle were well recorded. However, the deviation between the two measurements varied higher than expected. For low and medium throttle settings the deviation stayed within the $2N$ (Fig. 9b). For high throttle settings the deviation increased to $8N$. The overall error in measured thrust varied within 3%.

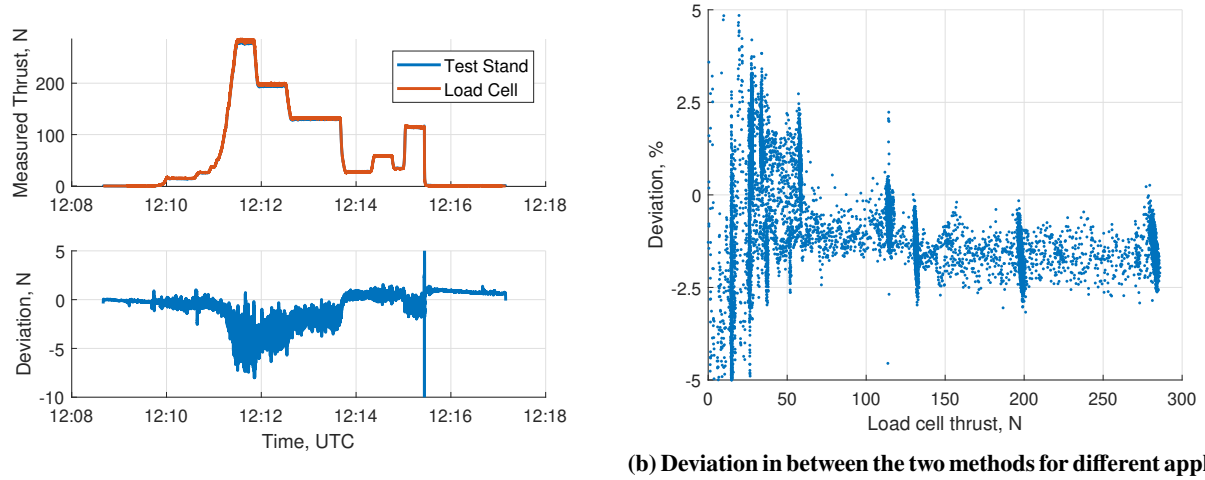

(a) Test profile and deviation in between the two methods.

(b) Deviation in between the two methods for different applied thrust, as a percentage of the applied thrust.

Fig. 9 Comparison of the thrust measurement received via calibrated thrust measurement system and a static thrust measurement stand.

The higher than expected error was attributed to multiple factors. Firstly, the static load stand was known to have high drift. This can be noticed in Fig. 9a, where after the measurement the thrust value, logged by the static stand, was not zero. The measurements were not corrected for the drift effects. Secondly, even though care was taken to mount the engine as level as possible, there was no system in place to confirm that the thrust axis is parallel to the axis of the measurement stand. The vertical measurements of the stand were not taken into account. This could have resulted in noticeable deviations, as the base of the engine stand was not yet reinforced and would bend. Additionally, temperature of the engine or the load cell was not measured during the test run. Therefore, it was not possible to tell if the deviation at higher thrust levels arise due to temperature. However, as the goal of the measurements with the static test stand was not to update the calibration, but rather to confirm it, the resulting deviations were interpreted as acceptable.

C. On-site calibration check

As the aircraft gets assembled and disassembled multiple times during a flight season [14] it was desired to have a confirmation that the system is still calibrated (especially the constant offset) right before each flight. It was speculated, that while the curve slope of the load cell would not change (as this would mean damage to the load cell), the constant offset might change slightly due to the surrounding features of the assembly. Therefore, another procedure for on-site calibration check was developed.

The procedure included tilting and rotating the assembled aircraft and use self-weight of the engine assembly together with the inertial measurements of the aircraft to compare the applied and measured load. The aircraft would be tilted nose down and nose up to apply longitudinal load on the load cell. It was then banked left and right to confirm the negligible (or measurable) influence of the roll angle on the measurement system. During the procedure, the same Eq. 2 was used to calculate the applied load.

The applied and measured loads are displayed in Fig. 10. The sum of the two signals, which in this case should be equal to zero, has a maximum amplitude of $2.6N$. This, converted into an error of measured thrust as described in section IV.A would result in $1.3N$.

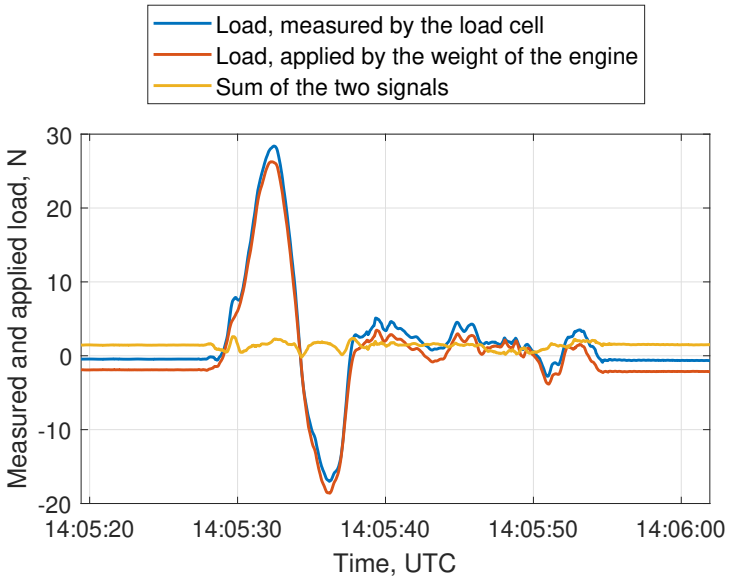

Fig. 10 Applied and measured load during the on-site calibration check. For clarity of comparison, the load applied by the engine is inverted. The sum of the two signals displays the effect of how data processing can compensate for changes in acceleration of the engine assembly.

The method has to be taken with care. Due to the dimensions of the demonstrator, the pitch angle is limited to roughly 25 deg, resulting in maximum applied load of around $30N$. In comparison, $100 - 150N$ range was assumed for steady level flight during a mission. Additionally, the load cell has a maximum load capacity of $700N$. Consequently it was assumed that the errors during the tilting procedure are of acceptable magnitude.

V. In-flight results

The system has been tested in-flight. Up to date, two test flights were done with the system. Results from one of them will are presented.

The flight profile with altitude and velocity is shown in Fig. 11a. The flight trajectory can be found in Fig. 11b. The flight was done on 10th of November, 2021 at Special Airport Oberpfaffenhofen (EDMO) in Germany. The main goal of the flight was to further extend the functionality of the autopilot, for which further details about the engine were needed. Therefore, many manually executed engine step inputs were done. Additionally, two test legs with different airbrake settings were tested, as well as different flap settings for take-off and landing.

Thrust was logged throughout the whole flight, including the engine start-up phase. Measured and modelled thrust is compared in Figure 12. For this comparison, thrust model based on engine revolutions, Mach number and altitude, developed during a different project was used [3]. Even though the two methods agree well at very low thrust values, an almost constant offset of $10N$ is seen during the rest of the flight. One reason for this might be that the engine model does not take the ambient temperature into account.

An extract of two throttle step inputs is shown in Figure 13. The lower sampling frequency of the engine revolutions, in comparison to the rest of the flight variables, can be noted. However, the thrust measurement system does follow changes in the engine spool speed well.

After reviewing the measured thrust, some trends of the system could not yet be explained. During the moments of high yaw rates, the system tend to have jumps in logged thrust, as can be seen in Figure 13. Even though the yaw rate is accounted for when changing the coordinate system of accelerations from the aircraft to the engine mount assembly, there still seems to be an unexplained component that influences the final measurement. Another unexplained increase in measured thrust is also marked. Both of these trends seem to appear only in highly unsteady motion. Further investigation for the cause will follow.

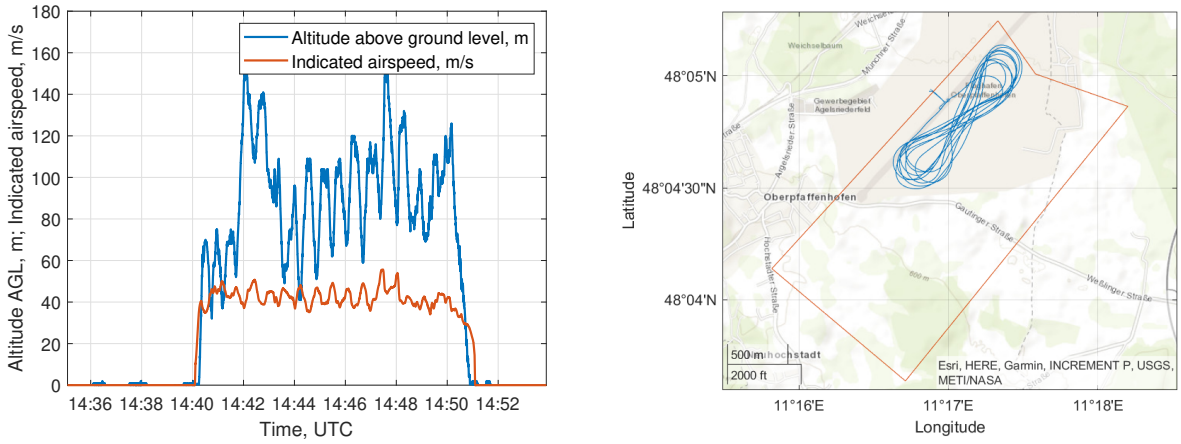

(a) Flight profile. **(b) Trajectory of the test flight.**

Fig. 11 Flight profile and flight trajectory for the test flight at Special Airport Oberpfaffenhofen. Throttle injection test points are visible from the altitude and airspeed plots.

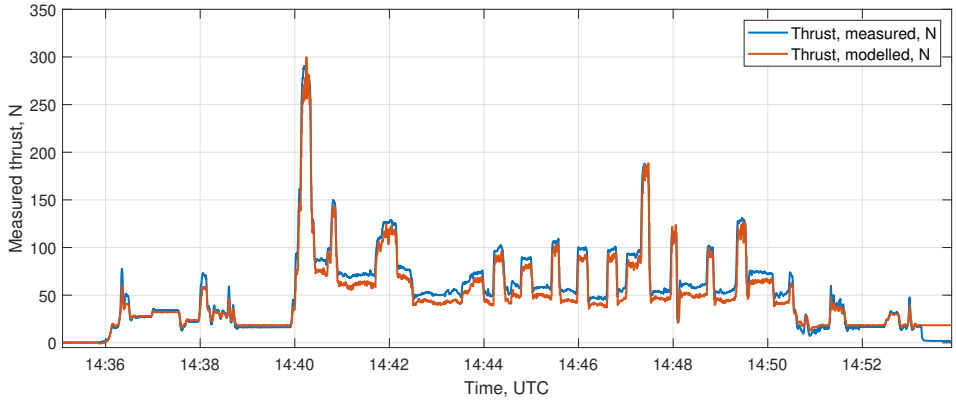

Fig. 12 Thrust measured during flight. For comparison, thrust modeled with respect to engine revolutions, Mach number and altitude is added [3].

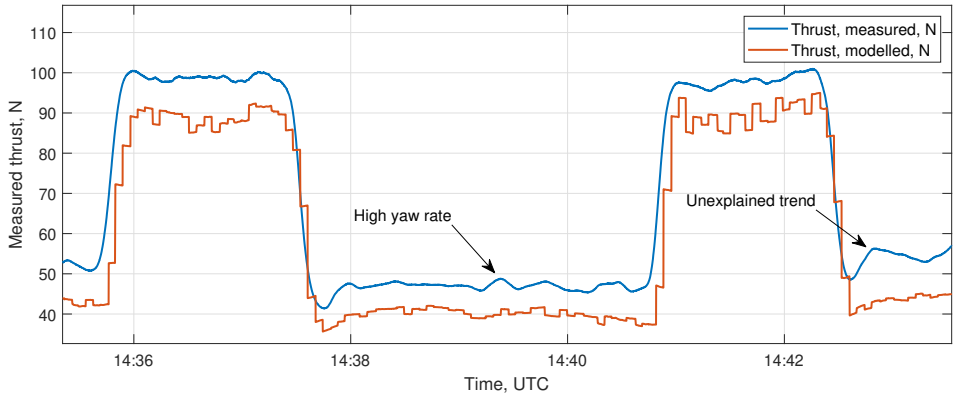

Fig. 13 Measured thrust during a throttle step input.

VI. Thrust modelling

It was desired to retrospectively model thrust for the T-FLEX flights that were conducted before the thrust measurement system was installed. For this reason, an update to the engine model was made, building on the data collected during the flight on 10th of November, 2021.

Data from half of the in-air time was extracted to derive the engine model. It was postulated that a thrust model based on the available engine throttle setting δF_T (actual vs maximum revolutions of the engine), ambient pressure p/p_0, stagnation temperature ratio T_{stag}/T_0, density ratio ρ/ρ_0, burner temperature ratio T_{burner}/T_{stag} and the Mach number M could be derived:

$$F_T/F_{max} = f(\delta F_T, p/p_0, T_{stag}/T_0, \rho/\rho_0, T_{burner}/T_{stag}, M) \tag{4}$$

Here F_{max} is the maximum engine thrust.

To derive the engine model from the sample data, nonlinear regression fit based on the Levenberg-Marquardt algorithm was used. The algorithm iterates the model coefficients starting from the initial values until lowest least-square error value is found. In this case, normalized thrust was used as the response variable.

Different combinations of predictors were iterated in order to reduce the complexity of the model. Finally, the postulated model was simplified to Eq. 5.

$$F_T/F_{max} = \beta_1 \delta F_T{}^{\beta_2}(1 - M^{\beta_3}) \tag{5}$$

The coefficients resulting from the nonlinear regression fit are provided in Table 5. The data used for modeling is presented in Fig.14a and the data used for validation of the model in Fig.14b. Model fit was determined as appropriate with $RMSE = 3.12N$. In the future, further updates of the model will be made.

Table 5 Coefficients of the nonlinear regression for the postulated engine model $F_T/F_{max} = \beta_1 \delta F_T{}^{\beta_2}(1 - M^{\beta_3})$.

	Estimate	Standard Error	t-Statistic	p-Value
β_1	1.1095	0.0007811	1420.5	0
β_2	3.8177	0.0009870	3867.9	0
β_3	0.7798	0.0015787	493.9	0

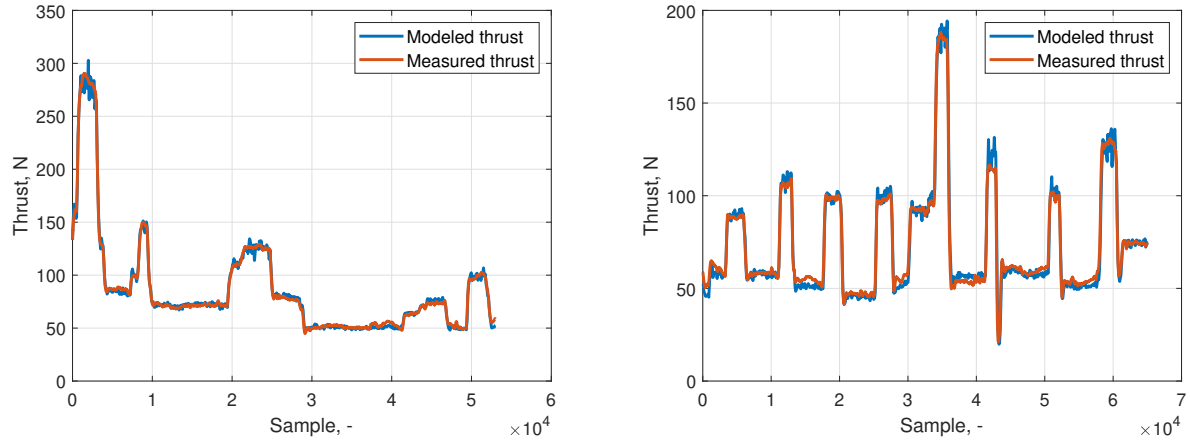

(a) Sample data used to create a thrust model of the engine. **(b) Validation of the created model.**

Fig. 14 Thrust modeling and validation from flight test data.

VII. Conclusion

A thrust measurement system was developed for a pylon-mounted miniature jet engine. The system was built and calibrated. During the static calibration with weights, simulated thrust accuracy of $0.64N$ was achieved. Higher

deviations were noted during the calibration check on the static test stand and during an on-site calibration check. However, due to the nature of the two calibration check methods, their accuracy was considered to be lower and the deviations are to be taken with care. Nevertheless, good response of the thrust measurement system was confirmed under operational conditions with the running engine.

The system was also tested in-flight. The system measurements did not present any unexpected behaviour during the steady flight. Some minor unexplained deviations were spotted during the unsteady segments. These, however, remained in the range of $2 - 5N$. Data gathered was seen appropriate to retrospectively model the thrust for the flights where no thrust measurement system was available.

To author's knowledge, this is the first time that thrust has been measured in-flight with high accuracy for a medium-sized unmanned aircraft.

Further investigation is needed to evaluate the nature of raw signal oscillations and the deviations during unsteady parts of the flight. It is expected that mounting an accelerometer on the hinged engine could improve the required corrections due to accelerations. Additionally, another static test run in the test stand should be done with the reinforced system to check the deviations during high-thrust segments. Finally, the same propulsion stack could be tested with an electric propeller engine to see if the high propeller vibrations induce high thrust measurement noise as observed by other authors.

Acknowledgments

The work presented has been conducted within the framework of projects FLEXOP (grant agreement No. 636307) and FLiPASED (grant agreement No. 815058) funded from the European Union's Horizon 2020 research and innovation program. The author J.B. would like to thank Mr. Pedro Alexandre Tonet Fleig, who designed, implemented and tested the measurement system, as well as Ms. Annina Metzner, who did further testing and investigation on the data. Additionally, J.B. would like to thank the rest of the T-FLEX flight test team for their contributions during flight tests with special thanks to Mr. Lars Nagel and Mr. Daniel Teubl who improved the logging system for the thrust measurements.

References

[1] Stahl, P., Sendner, F. M., Rößler, C., Hornung, M., and Hermanutz, A., "Mission and aircraft design of FLEXOP unmanned flying demonstrator to test flutter suppression within visual line of sight," *17th AIAA Aviation Technology, Integration, and Operations Conference, 2017*, American Institute of Aeronautics and Astronautics, Reston, Virginia, 2017. https://doi.org/10.2514/6.2017-3766.

[2] Nguyen, N., Ting, E., and Lebofsky, S., "Aeroelastic analysis of a flexiblewingwind tunnel model with variable camber continuous trailing edge flap design," *56th AIAA/ASCE/AHS/ASC Structures, Structural Dynamics, and Materials Conference*, 2015, pp. 1–28.

[3] Bougas, L., Rößler, C., and Hornung, M., "Design and experimental validation of a propulsion duct for a jet propelled low observable scaled UAV demonstrator," *17th AIAA Aviation Technology, Integration, and Operations Conference, 2017*, 2017, pp. 1–10. https://doi.org/10.2514/6.2017-4378.

[4] MIDAP Study Group, *Guide to In-Flight Thrust Measurement of Turbojets and Fan Engines*, ADVISORY GROUP FOR AEROSPACE RESEARCH AND DEVELOPMENT, 1979. https://doi.org/AGARD-AG-237.

[5] Davidson, T. W., "Measurement of net thrust in flight," *Journal of Aircraft*, Vol. 1, No. 3, 1964, pp. 107–113. https://doi.org/10.2514/3.43575.

[6] Conners, T. R., and Sims, R. L., "Full flight envelope direct thrust measurement on a supersonic aircraft," *34th AIAA/ASME/SAE/ASEE Joint Propulsion Conference and Exhibit*, Vol. 1998, No. July, 1998. https://doi.org/10.2514/6.1998-3872.

[7] Muhammad, H., Kuntjoro, W., and Sritjahjono, B. E., "In-Flight Thrust Determination by Load Measurement on the Engine Mounting System," *Proceedings of the 22nd International Congress of Aeronautical Sciences*, 2000, pp. 1–7.

[8] Martinez, A., "Design and manufacturing of a thrust measurement system for a micro jet engine," Master thesis, Linköping University, 2018.

[9] Sobron, A., "On Subscale Flight Testing Cost-Effective Techniques for Research and Development," Phd thesis, Linköping University, 2021. URL www.liu.se.

[10] Simavilla, E.-A. P., "Entwicklung und Implementierung eines on-board Schub- messsystems für UAV-Anwendungen," Master thesis, Technical University of Munich, 2020.

[11] Bronz, M., de Marina, H. G., and Hattenberger, G., "In-flight thrust measurement using on-board force sensor," *AIAA Atmospheric Flight Mechanics Conference, 2017*, 2017. https://doi.org/10.2514/6.2017-0698.

[12] Sartori, D., and Yu, W., "Experimental Characterization of a Propulsion System for Multi-rotor UAVs," *Journal of Intelligent and Robotic Systems: Theory and Applications*, Vol. 96, No. 3-4, 2019, pp. 529–540. https://doi.org/10.1007/s10846-019-00995-2.

[13] Bergmann, D. P., Denzel, J., Pfeifle, O., Notter, S., Fichter, W., and Strohmayer, A., "In-flight lift and drag estimation of an unmanned propeller-driven aircraft," *Aerospace*, Vol. 8, No. 2, 2021, pp. 1–16. https://doi.org/10.3390/aerospace8020043.

[14] Bartasevicius, J., Koeberle, S. J., Teubl, D., Roessler, C., and Hornung, M., "FLIGHT TESTING OF 65KG T-FLEX SUBSCALE DEMONSTRATOR," *32nd Congress of the International Council of the Aeronautical Sciences*, Shanghai, China, 2021, pp. 1–16.

[15] Sendner, F. M., Stahl, P., Rößler, C., and Hornung, M., "Designing an UAV propulsion system for dedicated acceleration and deceleration requirements," *17th AIAA Aviation Technology, Integration, and Operations Conference, 2017*, , No. June, 2017, pp. 1–13. https://doi.org/10.2514/6.2017-4105.

[16] Bauer, P., Anastasopoulos, L., Sendner, F. M., Hornung, M., and Vanek, B., "Identification and Modeling of the Airbrake of an Experimental Unmanned Aircraft," *Journal of Intelligent and Robotic Systems: Theory and Applications*, Vol. 100, No. 1, 2020, pp. 259–287. https://doi.org/10.1007/s10846-020-01204-1.

[17] Meddaikar, Y. M., Dillinger, J. K., Klimmek, T., Krüger, W. R., Wüstenhagen, M., Kier, T., Hermanutz, A., Hornung, M., Rozov, V., Breitsamter, C., Alderman, J., Takarics, B., and Vanek, B., "Aircraft aeroservoelastic modelling of the flexop unmanned flying demonstrator," *AIAA Scitech 2019 Forum*, , No. January, 2019. https://doi.org/10.2514/6.2019-1815.

[18] Koch, J., "Design and Development of a Jet Engine Thrust Measurement System for in-Flight Applications," Semester thesis, Technical University of Munich, 2020.

[19] "Interfaceforce Series SSM/SSM2 Technical Data," , 2020. URL www.interfaceforce.de.

[20] Fleig, P. A. T., "Improvement and Further Design of a Thrust Measurement System for In-Flight Applications on an Unmanned Aerial Vehicle," Master thesis, Technical University of Munich, 2020.

[21] Metzner, A., "Calibration and Testing of an In-Flight Thrust Measurement System for UAV Applications," Bachelor thesis, Technical University of Munich, 2021.